DIAGNOSE AND PREDICTION OF EROSION-CORROSION DAMAGE IN A PIPELINE TRANSPORTING REDUCED CRUDE OIL FROM THE HEATER TO THE VACUUM DISTILLATION TOWER

D. Ramajo[a]**, M. Raviculé**[b]**, R. Benini**[b]**, S. Marquez Damian**[a]**, M. Storti**[a] **and N. Nigro**[a]

[a]*International Center for Computational Methods in Engineering (CIMEC)*
INTEC-UNL-CONICET, Güemes 3450, Santa Fe, Argentina, dramajo@santafe-conicet.gov.ar
[b]*Centro de Tecnología Argentina (CTA), YPF, Baradero s/nro. 1925, Ensenada, Argentina,*
mravicules@repsolypf.com

Keywords: erosion-corrosion, oil refinery, CFD

Abstract. In this work a computational fluid dynamics study (CFD) was carried out with the aim to diagnose and mitigate the causes of damage in the pipeline that transport reduced crude oil from the heater to the vacuum distillation tower in the YPF Petrochemical plant at Ensenada. The reduced crude oil is mainly a two phase flow (liquid and vapor) that contains significant amounts of naphthenic acids. The operating conditions (temperature, flow velocity, annular flow, presence of drops and possibly solid coke particles) become it susceptible to erosive-corrosive attack, being the distillation tower frequently shut down.

The two phase flow was assumed as a homogeneous mixture and the drop-mean size and the net mass exchange from the annular film to the gas core were estimated. The Navier-Stokes equations and the Lagrangian particle tracking were applied to solve the mixture and the drop trajectories. Two damage mechanisms were investigated:

1- mechanical pick-up of material by drop-impact erosion enhanced by corrosion (*DIEC*)

2- loss of material by corrosion enhanced by relatively high flow velocity (*NAEC*).

Numerical results allowed identified regions of impact of drops (*DIEC*) and high wall shear stresses (*NAEC*) take place, these being in good agreement with the burst zones found in the pipeline. Nevertheless, due to the fact that there are no works reporting *DIEC* and scarce information about *NAEC*, the uncertainty about the damage mechanisms made impossible to accurately predict the erosion-corrosion rate. So, a comparative analysis in order to propose geometric modifications and operating condition changes to mitigate the damages was performed. It was proposed to modify a part of the pipeline, replacing several elbows by one large radius curve, reducing drop impacts and wall shear stresses. On the other hand, due to the corrosive composition of the reduced crude, a change on the duct material, replacing the currently carbon steel by stainless steel (317 L or similar), was also recommended based on bibliographic data.

1   INTRODUCTION

The worldwide increment of petroleum consumption had promoted the exploitation and refining of high acid crude oils. High-temperature naphthenic acid corrosion (*NAC*) and erosion-corrosion (*NAEC*) have become one of the major failure causes in petrochemical plants. In particular distillation units are highly susceptible to *NAEC*, especially where flow velocities are relatively high such as transfer lines, internals, heat exchangers and vacuum columns among others (Slavcheva et al., 1999). Vacuum distillation units are employed to process reduced crude oil by reducing operating pressure in order to increase the relative volatility of the key components of the crude; the higher the relative volatility, the more separable are the components. This connotes fewer stages in the distillation tower in order to effect the same separation between the overhead and the bottoms products. Vacuum distillation also requires operating temperature lower than the required for atmospheric distillation, thus being advantageous for many systems for which the products degrade or polymerize (cracking of the crude in this case) at elevated temperatures.

NAC and *NAEC* have been found in oil refineries for about 80 years but they are still far to be understood because of the ambiguous factors that dominates these phenomena. The factors related with the occurrence of *NAC* and *NAEC* can be roughly divided in two groups; those related to the chemical composition of oils and those concerning to the flow, the operating conditions and the construction materials. In the first group are the corrosively of crude oils (total acid number TAN), the activity, the boiling-point distribution and decomposition temperature of organic acids and other corrosive impurities such as sulfur species and chlorides. The factors included in the second group are the flow velocity, the degree of vaporization, the operating temperature and the susceptibility of materials to corrosion (Wu et al., 2004). Most of knowledge comes from field tests or in-plant failure reporters seeding poor and frequently inconsistent data. Regarding laboratory tests, usually there is a lack between laboratory and refinery conditions, especially for *NAEC* studies.

Erosion failures caused by the impact of particles must be also considered in petrochemical plants. Erosion by solid particles has been widely reported for numerous materials and test conditions (Mazumder et al., 2007, Zhang et al., 2007, Chen et al, 2006, Hamed and Tabakoff, 2006, Chen et al., 2004, Nokleberg and Sontvedt, 1995) However, solid particles are not expected in most processes but liquid drops are commonly found. Erosion by high-velocity drop impact (upper than 200 m/s) has been studied (Field, 1999, Nokleberg and Sontvedt, 1995), but erosion by relatively low-velocity drop impact (around 70 m/s) was not reported yet.

CFD has begun to be used for studying and predicting erosion (Nokleberg and Sontvedt, 1995; Forder et al., 1998; Chen et al., 2004; Mazumder et al., 2005; Brown, 2006; Chen et al., 2006; Zhang et al., 2007; Davis and Frawley, 2009). In this context, the current work is aimed to study, diagnose and prevent the failure causes on a vacuum distillation unit that is currently operating in the YPF Petrochemical plant at Ensenada. This unit was operated without problems for more than three decades but since three years ago it is frequently shutdown for reparation due to the loss of material and even the perforation in several points of the pipeline that connect the furnace to the vacuum tower, being the failures directly related with the recent processing of high-naphthenic-acid crudes.

Due to the lack of knowledge about *NAEC* and *DIEC*, the present work tries to investigate about feasible damage mechanisms that could cause the recurrent failure of the pipeline.

These mechanisms are evaluated with the assistance of CFD simulations in order to find qualitative concordance with the damage locations. CFD is also employed to assess some constructive modifications that would mitigate future damages.

2 METODOLOGY

2.1 General pipeline layout and damage-mechanism hypothesis

The studied pipeline have two twin lines, each line composed of four 8" ducts stretches (named secondary lines) that start from the furnace outlet and end in a 30" duct collector (named main line) that ends in the vacuum tower. Figure 1 shows two views of one of the four secondary lines and a part of the main line (white arrows point out the inlet). The main line as a blind extreme (at the right in figure) being the other extreme connected to the vacuum tower.
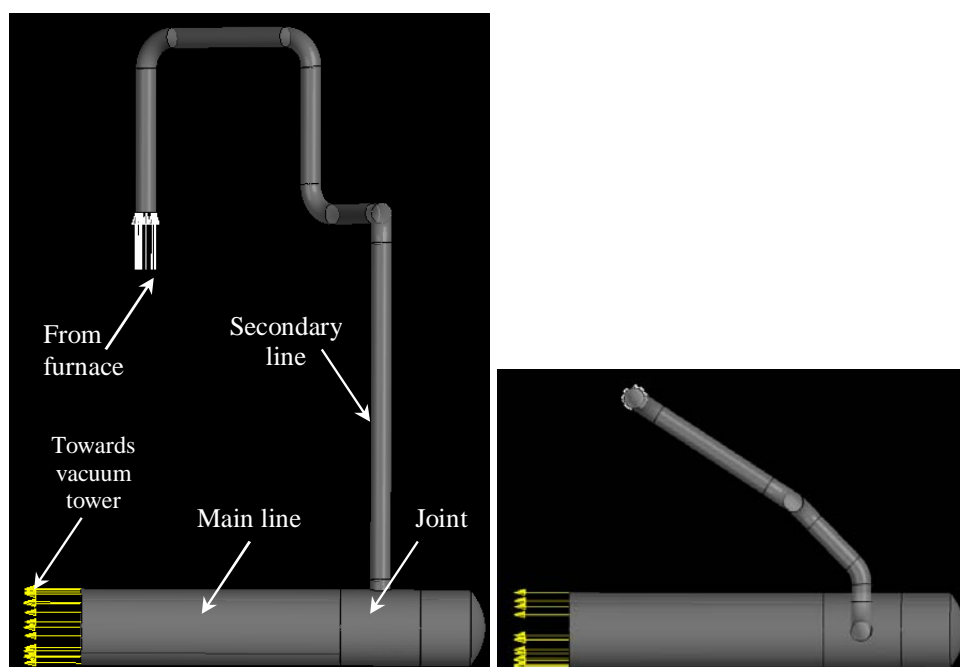

Figure 1. Geometry analyzed corresponding to one secondary line and a fraction of the main line of one of the two twin lines. Left: lateral view. Right: top view.

As was above mentioned Figure 1 only shows a part of one of the two twin lines that transports the reduced crude oil from the furnace to the vacuum tower. The real layout of each twin line consists of two pairs of secondary lines, each line in each pair separated 0.5 m and each pair separated from the other nearly 10 m. The total length of each one of the two main lines is around 46 m, while the length of each one of the eight secondary lines is approximately 7 m.

Figure 2 shows a picture of a part of one secondary line, corresponding to the end of a 90° elbow and the beginning of a straight duct (sample was cut along the mean plane). Note that the damaged zone is located just downstream of the welded seam. The elbow present

generalized corrosion (pitting) but only the straight duct shows severe damage. Similar failures can be found for all 90º elbows. Figure 2 also allow note the different thickness of the elbow and the straight duct. Elbows were fabricated of alloy steel with low content of molybdenum and chromium (0.53% Mo, 4.85% Cr, 0.40% Mn, 0.13% C, 0.02 Ni, 0.19 Si) while straight ducts were fabricated of carbon steel (0.01% Mo, 0.02% Cr, 0.53% Mn, 0.2% C, 0.02 Ni, 0.35 Si).

Figure 2. Typical failure downstream of a 90º elbow of a secondary line (Bilmes and Solari, 2008).

From preliminary studies it was identified the presence of corrosion by naphthenic acid in the surface damaged (Bilmes and Solari, 2008). On the other hand, due to the severity of the damage and the fast loss of material, damage can not be completely explained by *NAEC* and additional factor or factors must be considered as responsible of the damage. In this sense, the drop impact erosion-corrosion (*DIEC*) was considered. Then, the following scenario to explain the failures of the pipeline would be:

Naphthenic acid attack produces generalized corrosion, but those corrosion products subjected to high flow velocities or drop impact are quickly removed both by shear stress (*NAEC* mechanism) and by drop impacts. Based on this assumption, it is possible to predict that damage zones would be those wetted by the liquid phase and near abrupt direction changes.

2.2 Mechanical erosion models

Figure 3 schematizes the mechanism for ductile and brittle mechanical erosion caused by the impact of solid particles. The first known ductile erosion model was developed by Finnie (1960), based on the theory of micro-cutting. Later, it was demonstrated that micro-cutting is not the primary erosion mechanism in ductile materials, being the erosion caused by localized plastic strain and fatigue causing material removal from the metal surface. The maximum erosion rate is found for incidence angles (ϕ) lower than 25º. On the other hand, for brittle materials, impacting particles cause surface cracks and chipping of micro size metal pieces (Mazumder et al., 2007). The impact kinetic energy is the main erosion factor, thus being the maximum loss of material for incidence angles around $\phi = 90$º (Hamed and Tabakoff, 2006). Two interesting reviews about the evolution of erosion models can be found on works of Meng and Ludema (1995) and Finnie (1995).
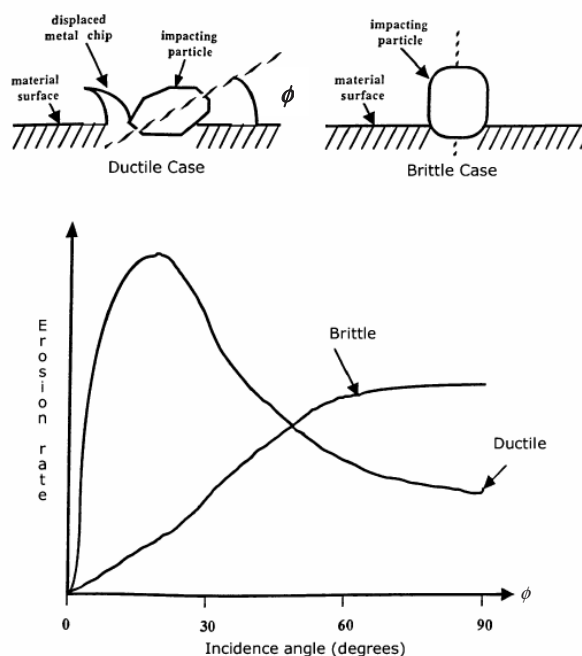

Figure 3. Mechanical erosion mechanisms and typical erosion rate versus incidence angle curves for ductile and brittle cases (Hamed and Tabakoff, 2006).

Figure 3 points out the importance of a correct election of the mechanical erosion mechanism; if the damage is caused under a ductile mechanism then the higher erosion damages would be found where low incidence angle particle impacts take place while for brittle erosion the maximum damages will take place where nearly normal particle impacts. It is clear that neither of both above mentioned mechanical erosion mechanisms can be directly responsible of the damage found in the pipeline. Consider the ductile mechanism; on the one hand, the eroded material (straight duct) is a relatively ductile material (carbon steel), but on the other hand drops are far to be sharp rigid shape particles (as the schematized in Figure 3). Now analyze the brittle mechanism; the eroded material is not a brittle material, but in this case the energy transfer by the drop impact mainly depends on

D. RAMAJO et.al.

the drop velocity, although it is obvious that a solid particle concentrates the impact energy in a smaller contact surface area. But on the other hand, corrosion produces cracking of the metal surface getting it brittle. So, the brittle erosion mechanism seems to be a bit more reasonable than the ductile one. As previously mentioned, bibliography does not help to clarify what is the failure mechanism. One thing is clear, the chronology of failures allows ensure that naphthenic acid corrosion play a crucial role in the failures.

In bibliography there are several mechanical erosion models formulated for solid-particle impact. Most of them are data correlations proposed for sand-steel or sand-aluminum experimental data (Hamed and Tabakoff, 2006; Mazumder et al., 2007). Correlations are quite similar, all considering the incidence angle, the particle velocity, a particle shape factor, one or several reference velocities and the incidence angle for maximum erosion (ϕ_{max}), being the last two parameters employed to define ductile or brittle erosion.

In this work the Grant and Tabakoff erosion model (Grant and Tabakoff, 1975) was employed to evaluate the erosion rate for ductile and brittle analysis. The general form of the erosion rate equation is the following:

$$E = f_\phi \left(\frac{V_p}{V_1} \right)^2 \cos^2 \phi \left(1 - \left(1 - \frac{V_p}{V_3} sen\phi \right)^2 \right) + \left(\frac{V_p}{V_2} sen\phi \right)^4 \tag{1}$$

where V_p is the particle impact velocity, V_1, V_2 and V_3 are reference velocities and f_ϕ is a function that depend on the incidence angle. The reference velocities are a set of parameters that depend on the particular combination of eroded and particle materials. As expected, there are few data for reference velocities and neither for carbon steel and liquid drops, so in this qualitative work steel-sand data were employed. Regarding the f_ϕ function, the following expression was employed:

$$f_\phi = \left(1 + k_2 k_{12} sen\left(\phi \frac{\pi/2}{\phi_{max}} \right) \right)^2 \tag{2}$$

being k_2:

$$\begin{aligned} k_2 &= 1 \quad if \quad \phi \le 2\phi_{max} \\ k_2 &= 0 \quad if \quad \phi > 2\phi_{max} \end{aligned} \tag{3}$$

where ϕ_{max} is the incidence angle corresponding to the maximum erosion. Eq. (1) to (3) can be used to represent both ductile and brittle erosion mechanisms depending on the chose parameters. Table 1 shows the parameters employed in this work for both erosion mechanisms and Figure 4 displays the erosion rate E obtained with different particle velocities (V_p) for the overall incidence-angle range (90º correspond to normal impact).

Mechanism	k_{12}	ϕ_{max} [deg]	V_1 [m/s]	V_2 [m/s]	V_3 [m/s]
Ductile	0.2	30	150	150	179
Brittle	0.2	90	250	135	279

Table 1. Parameters employed to represent ductile and brittle erosion mechanisms with the Grant and Tabakoff erosion model.
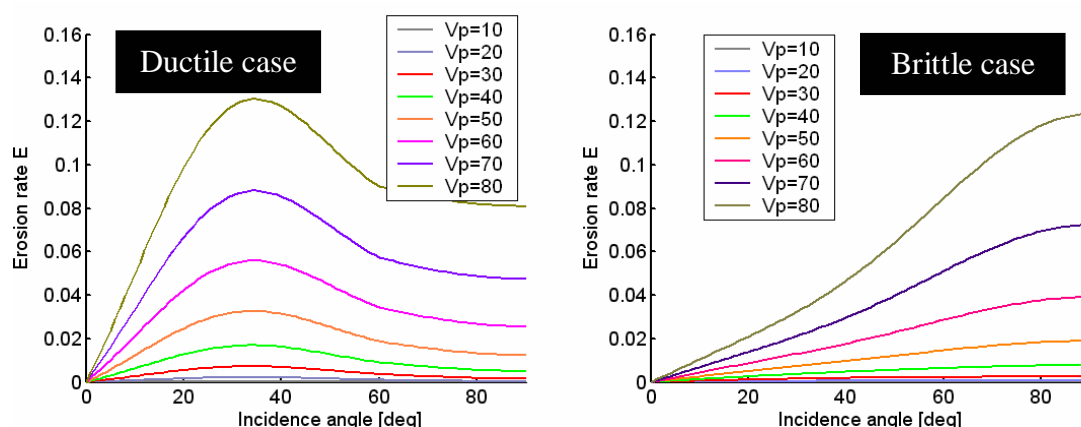
Figure 4. Erosion rate E as function of the incidence angle (ϕ) for several impact velocities. Left: ductile case. Right: brittle case.

The erosion rate E is a dimensional quantity, so to estimate the mass rate of material loss the erosion rate E must be multiplied by the mass of one particle and for the amount of particles that impacted at each position of the eroded material. That means, to obtain a representative erosion rate map over the surface the simulation period (Δt) must be enough and the amount of particles tracked (N_p) must be large. Then the erosion rate density (ERD) is obtained as a time average of the erosion rate density of all particles:

$$ERD = \frac{1}{\Delta t} \int_{t=0}^{t=\Delta t} E . \frac{m_T}{N_p} \tag{4}$$

where m_T is the total mass flow rate of particles.

Due to no experimental data about *DIEC* are available and erosion mechanism is not clearly determined, the scope of this work was to carry out a comparative/qualitative analysis of the pipeline failure based on correlations for sand-steel erosion under ductile and brittle mechanisms, although, as previously mentioned, the most possible scenario that explain failure seems to be brittle erosion mechanism.

2.3 Naphthenic acid corrosion (*NAC*) and erosion-corrosion (*NAEC*) models

Naphthenic acid corrosion (*NAC*) takes place when fluid containing naphthenic acids (*NA*) attacks a metallic surface. Although *NAC* only occurs in a narrow temperature window ranged from 200ºC to 400ºC, many relevant petrochemical processes also work in this temperature range (Garverick, 1994). A generic *NAC* reaction can be written as:

$$2nRCOOH + 2M \rightarrow 2M(RCOO)_n + nH_2 \tag{5}$$
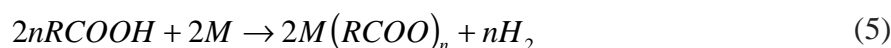
where R is the naphthenic radical, M is the susceptible metal and $M(RCOO)_n$ are the corrosion products. *NAC* can be roughly divided in four steps; 1- the transportation of *NA* molecules toward metal surface, 2- the absorption of *NA* at the active spots on metal surface, 3- the reactions at the active spots and 4- the spallation or dissolution of corrosion products from the surface. The increment of fluid temperature not only promoted the diffusion transportation of the *NA* molecules and desorption or dissolution of the corrosion products, but also aggravates the reaction due to its endothermic nature (Wu et al., 2004).

As was mentioned, temperature is one of the most factors affecting *NAC*. There is other key factor related with the steel chemical composition: the amount of molybdenum (Mo). Steels with Mo content higher than 3% show significant resistance against *NAC* attack. Moreover, the most serious *NA* attack is not by *NAC* but by *NAEC* (naphthenic acid erosion corrosion), that takes place when the fluid content *NA* flows at relatively high velocity over the metal surface (Wu et al., 2004; López et al., 2005). Figure 5 clearly shows the effect of both previously mentioned factors; *NAEC* is inversely proportional to the amount of Mo, being the effect of flow velocity negligible for Mo contents higher than 7%wt (Figure 5 on the left). On the other hand, Figure 5 on the right shows the drastic effect produced by fluid velocity on the erosion-corrosion rate over carbon steel. Figure 5 is also useful to note the significant increment on erosion-corrosion rate with temperature (Wu et al., 2004; Qu et al., 2006).
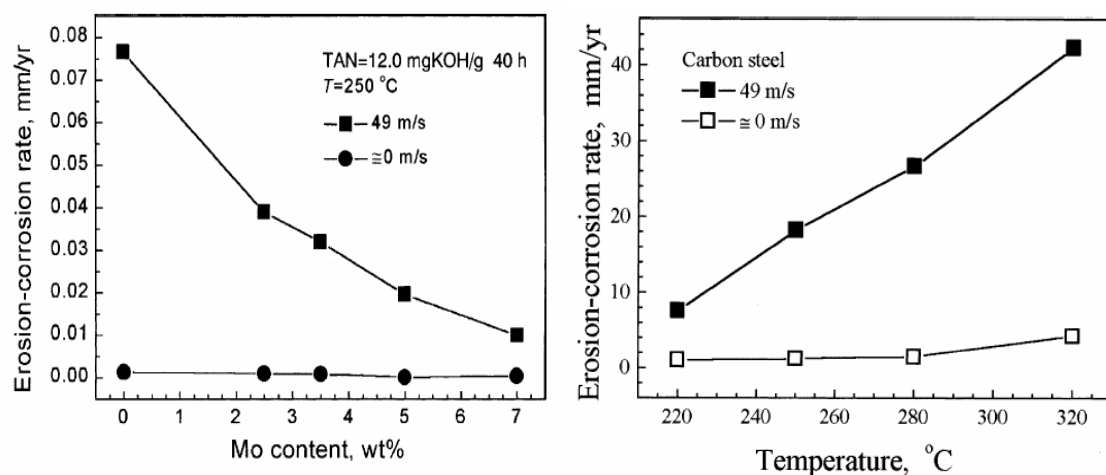

Figure 5. Naphthenic acid erosion-corrosion *NAEC* for a tangential flow at 0 and 49 m/s (Wu et al., 2004). Left: stainless steels with different content of molybdenum. Right: carbon steel.

2.4 Computational models

Due to the complexity involved in simulating multiphase annular flow, the two-phase flow was assumed as one-phase with mixture properties for density and viscosity. The Navier-Stokes unsteady incompressible equations were solved, models were considered as isothermal and phase change (evaporation) was not taking into account along the pipeline. The fraction of vapor was assumed constant it being the average along the corresponding simulated stretch. Although crude vapor clearly is a compressible fluid, due to the relatively low flow velocity the compressible effects become negligible, therefore incompressible formulation was appropriate in this context. Turbulence was modeled through a standard k-ε model. Simulations were unsteady, so a suitable time step was obtained through a time-convergence study, being this 5×10^{-4} seconds. Models were solved using distributed computing facilities over several processors in a Beowulf cluster (Storti et al., 2002; Sonzogni et al., 2002).

Two computational models were solved:

1-firstly were studied local models of the join between the secondary and the main line (named joint models). Three geometries were analyzed, the first one corresponding to the

current geometry of the most compromised pair of secondary lines (closer to the blind top of the main line). The second one analyzing the effect of separate one secondary line from the other (simulation of an isolated secondary line). Finally, the third model to evaluating the convenience of change the incidence angle from 90º to 45º.

2-secondly it was studied the overall geometry of the current secondary line along with a fraction of the main line (named overall models), as showed in Figure 1. After that, a modified secondary line, changing the six elbows for a unique large curve (this modification will be presented later in Figure 14) was also simulated.

2.4.1 Drop entrainment

Figure 6 shows the current secondary line connecting the furnace with the main line. As showed, the secondary lines have four 90º elbows and one 45º elbow. Six straight ducts complete the secondary line.
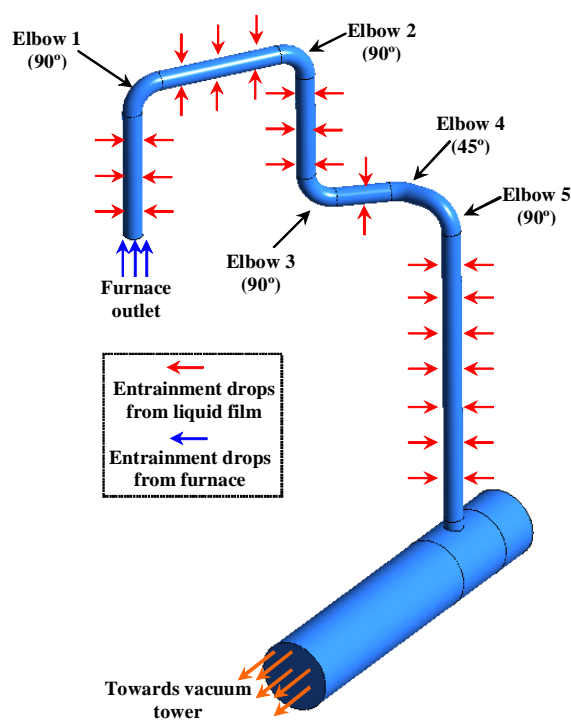

Figure 6. Computational model showing the drop entrainment zones.

From a 0/1-dimensional simulator (0/1-D) refinery data the entering flow is a multiphase (liquid-vapor) annular mist flow with a mass flow rate of 7.1 kg/s. The liquid/vapor ratio is not fixed along the pipeline due to pressure decreases towards vacuum tower, causing liquid evaporating. From 0/1-D data, at the beginning of the secondary lines (furnace outlet) around 25.7%wt of the mixture is vapor, reaching around 41%wt at the end of the secondary lines, being the total mass flow rate of the mixture through each secondary line 7.1 kg/s. Table 2 reports the operating conditions predicted by the 0/1-D simulator at the inlet and outlet of the secondary lines.

Secondary line	Pressure (Pa)	Temperature (K)	Vapor mass fraction	Viscosity* (Pa s)	Density* (kg/m^3)	Mean velocity (m/s)
Inlet	48950	659	0.257	1.67x10^{-5}	4.33	41.1
Outlet	22752	654	0.41	1.58x10^{-5}	2.71	89

Table 2. 0/1-D data at the beginning and the end of the secondary lines. *Correspond to mixture values calculated by mixture law.

Assuming that drop-impact erosion corrosion (*DIEC*) is caused by drops traveling in vapor core. Then, the drop size and the amount of drops can be roughly estimated by using correlations obtained from annular flow experiments. These correlations allow find the net drop entrainment rate ($\dot{m}_{der}$) of drops that continuously migrates from the slow liquid film (flowing at walls) to the fast vapor core. The entrainment phenomena is extremely complex due to liquid film is a very thin layer (in this case thickness estimations are around 0.5 mm). In this thin film the liquid velocity increases from zero at the walls to near the vapor core velocity at the liquid-gas interface. In this scenario, small drops are continuously removed and dragged from the film surface to the vapor core while other drops return to the film. The mass balance at liquid-gas interface results in a net mass transfer from the film to the gas core (named entrainment rate) (Ishii, 1975, 1976; Fukano and Furukawa, 1998; Ambrosini et al., 1991; MacGillivray, 2004; Hazuku et al., 2007). From correlations (MacGillivray, 2004; Hazuku et al., 2007) it was found that the average entrainment rate is around $\dot{m}_{der}$ = 0.075 kg/s for each meter of duct, being the drop size around 200 microns. Returning to Figure 6, in this are schematized (by means of red arrows) the locations were drops are injected to the flow. Drops were injected at the straight ducts of the secondary line and at the inlet of the line (considering that the vapor core content and initial amount of drops equal to $\dot{m}_{der}$).

2.4.2 Drop tracking

The trajectory of each drop was obtained by solving the summation of forces over a particle (Lagrangian particle tracking). In general, for a generic particle (drop, bubble, or solid particle) efforts from drag, pressure gradients caused by the acceleration of the fluid surrounding the particle, acceleration of the fluid in the volume occupied by the particle (virtual mass efforts), buoyancy and centripetal and Coriolis forces (rotating frame systems) are computed. But, specifically for drops moving in a non-rotating gas media, only drag forces become significant. In this work, the well known and commonly employed Schiller-Naumann drag model (1933) was employed.

For solid particle impact, especially for sand impacting solid walls there is much information about the particle behavior and restitution coefficients. But, as imagine the behavior of a drop after it impacts a wall is completely uncertain. Drops can stick to the wall, break into many smaller drops, or a fraction of a drop can stick to the wall while the other fraction separates from the wall as smaller drops. All these possibilities get hard difficult the prediction of drop trajectories after impacting. For this reason, the election of suitable restitution coefficients for tangential and normal impacts is almost impossible. Due to the lack of knowledge in this sense, in this work the restitution coefficients were taken equal zero, that means, drops loss all their kinetic energy when they touch a wall.

2.4.3 Model discretization

Hybrid meshes composed of tetrahedric and edge elements were employed for the overall and the joint models. Straight ducts and elbows were discretized with edges and tetrahedric elements were employed around the joint between the secondary and the main line. Figure 7 shows some details about the domain discretization with edge elements. The cross transversal discretization was performed with triangular elements that were extruded along the ducts and elbows. That allows get a good refining along the cross transversal direction without increase the amount of elements along the axial direction, being mesh sizes around $5.7x10^5$ elements and $1.3x10^5$ nodes for the joint models and around $1.9x10^6$ elements and $9.3x10^5$ nodes for the overall models.
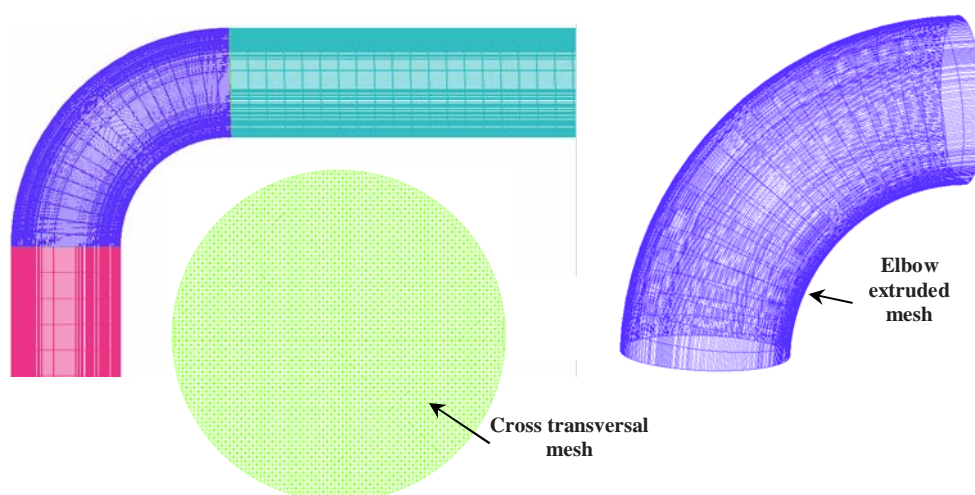

Figure 7. Detail of the extruded mesh employed for meshing the secondary duct and elbows and cross transversal discretization.

3   RESULTS

3.1 Study of the joint between the secondary and the main line

3.1.1 Mechanical erosion analysis

The four secondary lines of each main line have the same flow, but the pair closer to the blind extreme of the main line presents the worst condition for erosion taking into account that the flow entering for the other pair is dragged by the upstream flow. For this reason it was studied the pair nearest to the blind end of the main duct. Figure 8 shows the particle trajectories of drops entering with the flow along with others injected from the secondary duct wall obtained for three models: 1- firstly the current geometry (two second lines separated for 0.5 m one from the other) and for two proposal geometries, 2- secondly considering that the distance between the secondary lines is too enough that there is no influence between lines (modeling an isolated line) and 3- thirdly also considering a unique

line but for an incidence angle of 45º. As noted from Figure 8, a short part of the total secondary line was considered for this local analysis and symmetric models were employed.
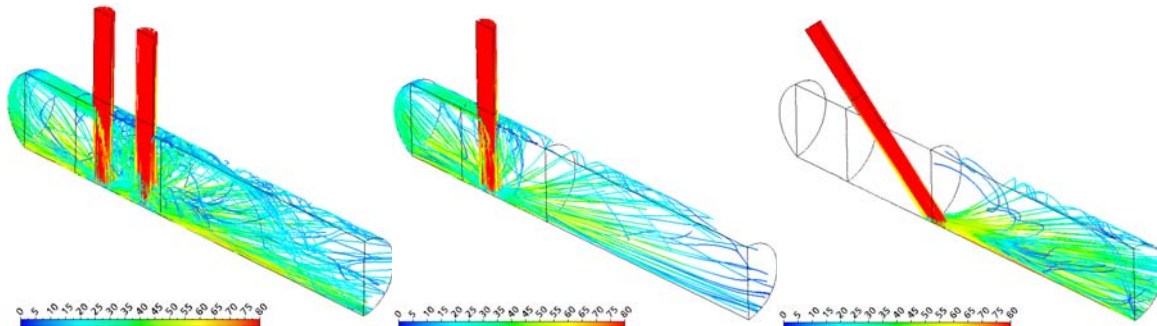

Figure 8. Particle trajectories for three models of the secondary line to main line connection. Left: Current geometry. Center: considering only one line. Right: considering only one line with an incidence angle of 45º.

Note from Figure 8 that drops enter with velocities upper than 80 m/s (due to the high vapor fraction at the end of the secondary line) and trajectories are strongly straight.
Figure 9 shows the flow velocities for the three models. Note that flow velocity is slightly reduced by the duct expansion at the main line. For the first two models, a fraction of the entering flow is directed towards the blind end of the main line producing a recirculating zone.
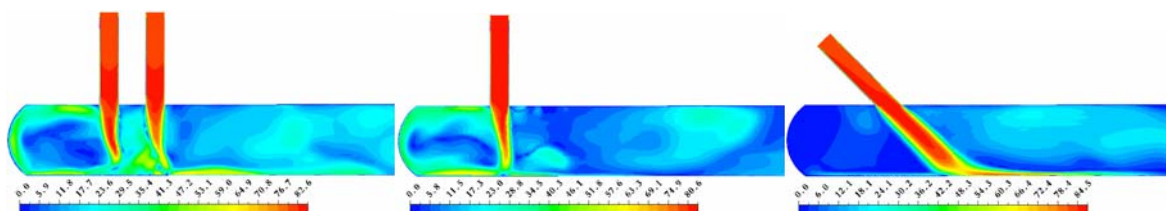

Figure 9. Flow velocity for three models of the secondary line to main line connection. Left: Current geometry. Center: considering only one line. Right: considering only one line with an incidence angle of 45º.

Figure 10 shows the erosion rate density *ERD* [mm/year] obtained for the three models applying the brittle mechanism model. Results correspond to locally spatial average around each one of 30 monitoring points at the main duct wall over the mean plane (see the sketch in Figure 10 on the center). Point 1 is located at 0.3 m at the left from the left secondary line axis and point 30 at is located at 0.45 m at the right from the right secondary line axis. Note that for the first model the second *ERD* peak is significantly lower than the first one due to the upstream flow. The *ERD* caused by the drop injected at walls is notoriously lower than that caused by the drops entering with the flow at the inlet. Comparing results for the first and the second models it is clear that increase the distance between the secondary lines has not profit because interaction between jets is negligible. The reduction

of *ERD* obtained by changing the incidence angle of the line from 90º to 45º is expected since the brittle erosion model has maximum erosion rate for normal incidence angle. Moreover, for the third model drops travel a large distance before impact the wall, so their velocity is slightly reduced. Of course, *ERD* reduction directly depends on the election of the erosion model; for the ductile model results are opposite and the better condition is obtained for normal incidence angle.
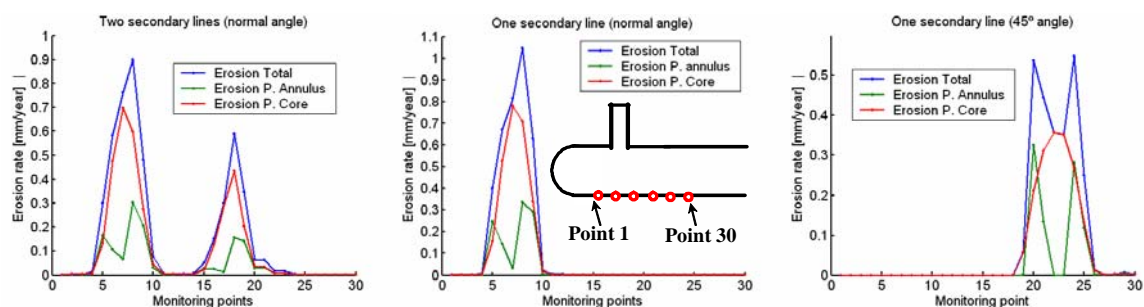

Figure 10. Erosion rate (brittle model) at monitoring points located at the bottom main-line wall. Left: Current geometry. Center: considering only one line with an incidence angle of 90º. Right: considering only one line with an incidence angle of 45º.

3.1.2 Erosion-corrosion analysis

Naphthenic acid erosion-corrosion (*NAEC*) was estimated from an indirect point of view, analyzing the wall shear stress. High wall shear stresses are directly related with high flow velocity, it being recognized as one of the indicators of potential *NAEC* damage. Figure 11 shows the wall shear stress for the three models previously presented. The actual geometry shows the maximum stresses at the main duct wall. For models with normal incidence angle wall shear stresses also appears at the blind top of the main line end. Wall shear stresses for the third model are also significant and, even the zone with high shear stress is increased.
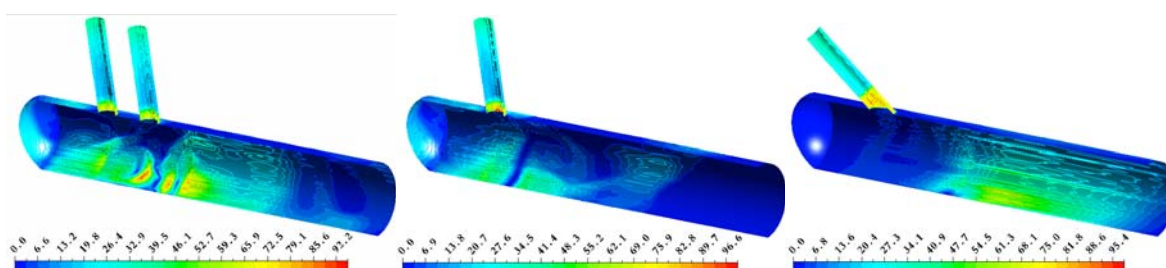

Figure 11. Wall shear stress for the three models. Left: Current geometry. Center: considering only one line with an incidence angle of 90º. Right: considering only one line with an incidence angle of 45º.

Summarizing, wall shear stress patterns are similar for the three models analyzed, so *NAEC* is not reduced by the proposed geometric changes. It is expected that the lower the incidence angle of the secondary line the lower the wall shear stresses, but on the other

hand that implies a significant change on the upstream flow direction before the joint by introduce an additional 90º elbow that possibly will suffer *NAEC* and *DIEC*.

One geometric modification that would reduce *NAEC* is to expand the secondary duct at the joint to locally reduce the flow velocity without introduce strong changes in the pressure drop of the line. For example, to increase the duct diameter 2 inches lead a cross sectional area increment of around 56% with a similar reduction of the flow velocity. Duct diameter increments only can be locally considered due to pressure drop must holds almost the same. A change of the duct diameter of the overall line will reduce the pressure drop of the line increasing the pressure inside the furnace and along the line (pressure at the vacuum tower is fixed for processing reasons) causing more vaporization and of course a sensible increment of flow velocity.

3.2 Study of the overall secondary line

Figure 12 shows results corresponding to the overall model. In figure are consigned the results for mechanical erosion *DIEC* (only the brittle model was considered) and due to wall shear stresses (*NAEC*). Note that the locations of high *DIEC* are concentrated around the elbows. As expected, there is a significant influence of the methodology for particle injection on predicted *DIEC*. For elbow 1 the erosion zone is significantly more extended than for the others. That is caused by the presence of drops entering with the flow. Due to the null restitution coefficients chose, drops loss all their kinetic energy after the first impact. It is necessary to note that a unique drop size was employed for simulations. Although the employed drop size was calculated from correlations and models for annular flow, it represents the mean drop size and a size distribution will be considered for more precise estimations. Exploratory simulations (not reported in this work) allowed find that variations around the chose drop size (200 microns) has a strongly influence on drop trajectories. Drops with sizes smaller than 50 microns are almost completely dragged by the fluid while those larger than 500 microns are little deviated by the flow in the elbows and follow straight trajectories. From this, the obvious consequence of introduce a drop size distribution is the increment on the eroded zone predicted.
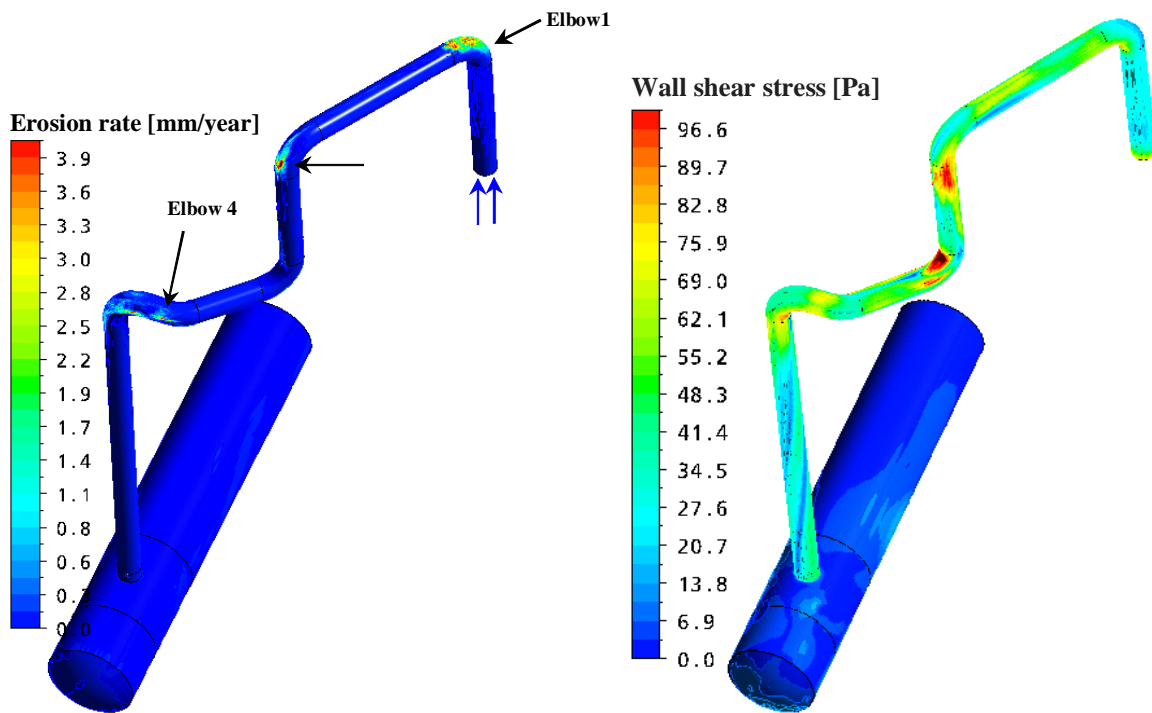
Figure 12. Results for the current geometry. Left: Erosion rate. Right: wall shear stress.

Figure 13 shows the drop trajectories along different stretches of the secondary line. Note that particles trend to go ahead at elbows. As was mentioned, drops are basically affected by drag forces and also for the pressure gradient in the curve radial direction at elbows.
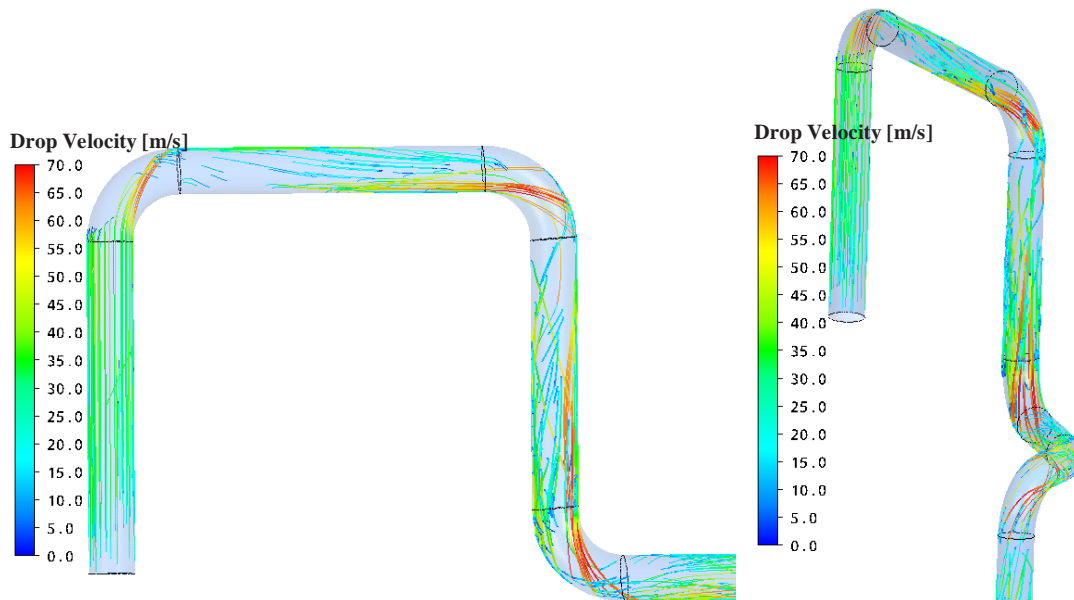

Figure 13. Drop trajectories in some stretches of the secondary line.

3.3 Geometric modifications

With the aim to reduce the impact of drops and maybe avoid the rupture of the annular flow in the elbows, a geometry modification changing the five elbows of the secondary lines by a unique large radius curve was proposed. Figure 14 shows the erosion rate (related to *DIEC*) and the wall shear stress (related to *NAEC*) for the new design. Regarding the drop impacts, they are significant for the first part of the curve, but then *ERD* decreases around 10 times for the rest of the line. Wall shear stress holds more homogeneous, although peak values are lower than that found for the current line geometry although the mean value results similar.

The common sense allows think that greater curve radius will reduces erosion by minimizing drop impacts and hold the annular film added to the walls. In fact, the plant experience shows that the straight duct stretches only show general corrosion attack (pitting). Moreover, the proposed curve to replace the multi-elbow secondary lines could have radius 50% larger than the considered in the current study, and the reduction on pressure drop caused by replace the short radius elbows could be compensated by enlarging the secondary lines.
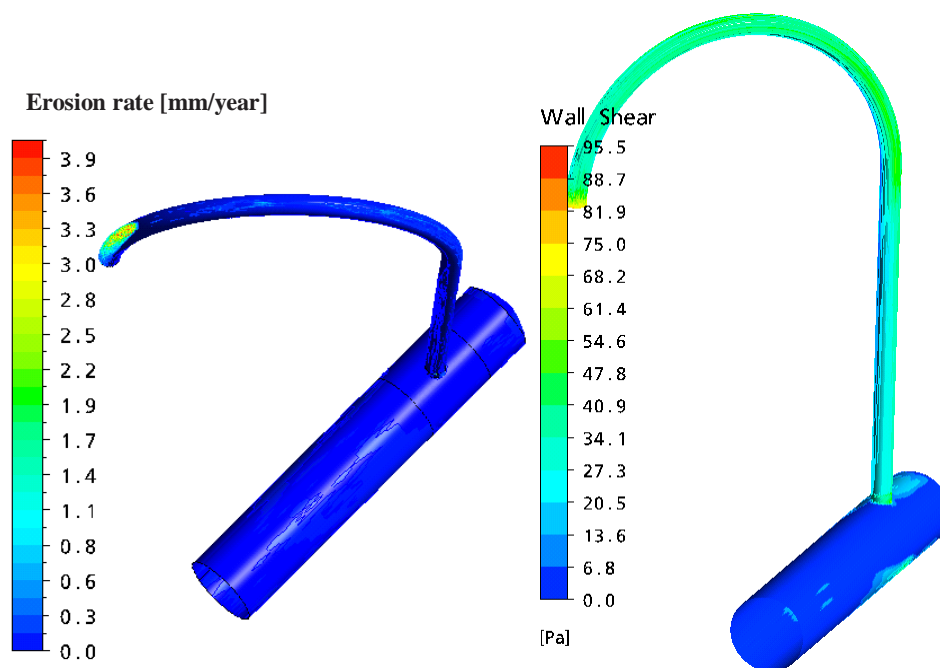

Figure 14. Results for the modified geometry. Left: Erosion rate density *ERD*. Right: wall shear stress.

4   CONCLUSIONS

From the results obtained in this work more questions than answers can be reached. As explained in the Introduction, it is clear that erosion-corrosion in petrochemical plants is becoming more and more relevant and poor efforts have been devoted to develop computational tools for predicting it. Experimental data is scarce and limited to specific test conditions and in many times not enough rigorous to extract general conclusions. The complexity of the erosion-corrosion mechanism become more complex for systems like the

above analyzed, where a multiphase flow, composed of gas, liquid drops and maybe solid particles (e.g. coke) flow at relatively high velocity. Experimental data refers to one-phase flows, but for multiphase annular flows the intermittent wetting, often produced downstream curves (where liquid film detaches) adds an additional uncertainly effect. Complex phenomena like annular flow, drop entrainment, drop coalescence and break up, drop-size distribution, dynamic of drops after impacting with walls and the stability of the very thin liquid film at walls must be taken into account.

Regarding the direct drop-impact erosion corrosion mechanism (*DIEC*), bibliography is not available, and due to erosion is only produced under corrosive environment, much experimental effort will be necessary to understand the overall mechanism.

Regarding the industrial system analyzed, it is clear from bibliography data that carbon steel as low resistance to *NAC* attack and even less to *NAEC*. So, a metallurgic change of the pipeline material to one with molybdenum contents upper than 3% (317 L or similar) seems to be the simplest option to minimize erosion-corrosion attack. On the other hand, some geometric changes as change the multi-elbow secondary line by a unique large radius curve and locally expand the secondary line at the extreme where it joint with the main line also show promissory profits.

5 ACKNOWLEDGEMENTS

6 REFERENCES

Adler W., Erosion: Prevention and Useful Application, *ASTM publication*, 1979.

Ambrosini W., Andreussi P. and Azzopardi B., A physically based correlation for drop size in annular flow, *I. J. Multiphase Flow*, 17:497-507, 1991.

Bilmes P., Solari M., Análisis de falla de un trazo de caño y niple del ramal de salida carga del horno BA-101, *Informe Técnico*, 2008.

Brown G., Use of CFD to predict and reduce erosion in an industrial slurry piping system, *fifth Int. Conference on CFD in the Process Industries*, Melbourne, Australia, 2006.

Chen X., McLaury B., Shirazi S., Application and experimental validation of a computational fluid dynamics (CFD)-based erosion prediction model in elbows and plugged tees, *Computers & Fluids*, 33:1251-1272, 2004.

Chen X., McLaury B., Shirazi S., Numerical and experimental investigation of the relative erosion severity between plugged tees and elbows in dilute gas/solid two-phase flow, *Wear*, 261:715-729, 2006.

Davis C., and Frawley P., Modelling of erosion-corrosion in practical geometries, *Corrosion Science*, 51:769-775, 2009.

Finnie I., Erosion of surfaces by solid particles, *Wear*, 3:87-103, 1960.

Field J.E., ELSI conference: invited lecture Liquid impact: theory, experiment, applications, *Wear*, 233-235:1-12, 1999.

Finnie I., Some reflections on the past and future of erosion, *Wear*, 186:1-10, 1995.

Folder A., Thew M. and Harrison D., A numerical investigation of solid particle erosion experienced within oilfield control valves, *Wear*, 216:184-193, 1998.

Fukano T. and Furukawa T., Prediction of the effects of liquid viscosity on interfacial shear stress and frictional pressure drop in vertical upward gas-liquid annular flow, *I. J. Multiphase Flow*, 24(4):587-603, 1998.

Ishii M. and Grolmes M., Inception criteria for droplet entrainment in two-phase concurrent film flow, *AIChE J.*, 21(2):308-318, 1975.

Ishii M., One-dimensional drift flux modeling: one dimensional drift velocity of dispersed flow in confined channel, *ANL Report,* 76-49, 1976.

Garverick L., Corrosion in the Petrochemical Industry, *ASTM publication*, 1994.

Grant G. and Tabakoff W., Erosion prediction in turbomachinery resulting from environmental solid particles, *J. Aircraft*, 12,5:471-478, 1975.

Hamed A., Tabakoff W., Wenglarz R., Erosion and Deposition in Turbomachinery, *J. Propulsion and Power*, 22,2, 2006.

Hazuku T., Takamasa T., Hibiki T. and Ishii M., Interfacial area concentration in annular two-phase flow, *I. J. of Heat and Mass Transfer*, 50:2986-2995, 2007.

MacGillivray R., Gravity and Gas Density Effects on Annular Flow Average Film Thickness and Frictional Pressure Drop, *MSc. Thesis*, 2004.

Mazumder Q., Shirazi S., McLaury B., Shadley J. and Rybicki E., Development and validation of a mechanistic model to predict solid particle erosion in multiphase flow, *Wear*, 259:203-207, 2005.

Meng H. and Ludema K., Wear models and predictive equations: their form and content, *Wear*, 181:443-457, 1995.

Nokleberg L., Sontvedt T., Erosion in choke valves-oil and gas industry applications, *Wear*, 186:401-412, 1995.

López D., Congote J., Cano J., Toro A., Tchiptschin A., Effect of particle velocity and impact angle on the corrosion-erosion of AISI 304 and AISI 420 stainless steels, *Wear*, 259:118-124, 2005.

Qu D.R., Zheng Y.G., Ping H.M. Yao Z.M., Ke W., High temperature naphthenic acid corrosion and sulphidic corrosion of Q235 and 5Cr1/2Mo steels in synthetic refining media, *Corrosion Science*, 48:1960-1985, 2006.

Schiller L., and Naumann A., Über die grundlegenden berechungen bei der schwerkraftaufbereitung, Vereines Deutscher Ingenieure, 77:318-320, 1933.

Slavcheva E., Shone B., Turnbull A., Review of naphthenic acid corrosion in oil refining, *Br. Corrosion J.*, 34:125-131, 1999.

Sonzogni, V., Yommi, A., Nigro, N., and Storti, M., A parallel finite element program on a Beowulf Cluster, *Advances in Engineering Software*, 33:427-443, 2002.

Wu X., Jing H., Zheng Y., Yao Z., Ke W., Erosion-corrosion of various oil-refining materials in naphtenic acid, *Wear*, 256:133-144, 2004.

Wu X., Jing H., Zheng Y., Yao Z., Ke W., Resistance of Mo-bearing stainless steels and Mo-bearing stainless-steel coating to naphthenic acid corrosion and erosion-corrosion,

Corrosion Science, 46:1013-1032, 2004.

Zhang Y., Reuterfors E., McLaury B., Shirazi S., and Rybicki E., Comparison of computed and measured particle velocities and erosion in water and air flows, *Wear*, 263:330-338, 2007.